Engineering with Computers
https://doi.org/10.1007/s00366-021-01387-7

ORIGINAL ARTICLE

Effect of viscoelastic properties of polymer and wavy shape of the CNTs on the vibrational behaviors of CNT/glass fiber/polymer plates

Farzad Ebrahimi[1] · **Reza Nopour**[1] · **Ali Dabbagh**[2]

Received: 28 January 2021 / Accepted: 17 March 2021

Abstract
Carbon nanotube (CNT)-reinforced polymer nanocomposites possess marvelous stiffness and strength as well as viscoelastic nature due to the time-dependent properties of the polymers. Hence, adequate knowledge about their rheological behavior is required if it is aimed at using such nanomaterials in design of aerospace structures. Present manuscript is arranged to account for the time-dependency of the polymer as well as wavy shape of the CNTs while tracking the vibrational responses of multi-scale hybrid nanocomposites for the first time. To this purpose, a mixture of the modified Halpin–Tsai model and mixture's rule is used for the homogenization process. According to the dynamic form of the virtual work's principle, the governing equations of the problem will be attained based on a higher-order shear deformable plate theorem to consider for thick structures. In addition, the Navier's analytical solution is implemented to extract the system's natural frequency for simply-supported plates. The findings of this paper indicate on the fact that the vibration suppression in the nanocomposite structures can be delayed if a high value is assigned to the characteristic relaxation time of the polymer. Besides, it is illustrated that hybrid nanocomposites consisted of wavy CNTs (i.e., corresponding with more realistic case) cannot provide ideal frequencies related to the nanocomposites manufactured from straight CNTs.

Keywords Multi-scale hybrid nanocomposite · Viscoelastic material · Waviness · CNT-reinforced polymer · Vibration analysis

1 Introduction

Carbon nanotubes (CNTs) discovered in 1991 [1] have shown huge potential in various applications since they have excellent mechanical and electrical properties [2, 3]. CNTs have absorbed interest and are extensively used in nano-engineering applications due to their properties such as superior ultimate stiffness and strength, high slenderness ratio, light weight, and high thermal conductivity [4]. According to the above reasons and motivated by the capabilities of CNT-reinforced (CNTR) polymers in the field of structural mechanics, many of the researchers made efforts toward providing reliable data concerning both static and dynamic characteristics of CNTR nanocomposite structures [5–35]. In the aforementioned Refs., the focus was on the structural behavior of the nanocomposite structure and lower attention is dedicated to the material's features. In other words, the CNTR polymer was treated as a simple polymer composite whose material properties can be calculated by the means of the conventional methods available in the composite materials' open literature. However, some studies can be found among which more physical data are reported in them. For example, the impact of the mostly probable wavy shape of the CNTs, caused by high slenderness ratio of them, their topological defect, and van der Waals (vdW) forces between individual CNTs [36, 37], on the stiffness of the CNTR polymers with low CNT loading was covered in the framework of a semi-empirical analysis accomplished at the beginning of the 2010s [38]. After about a half of a decade, a theoretical position-dependent functionally graded (FG) model for the

✉ Farzad Ebrahimi
febrahimy@eng.ikiu.ac.ir

[1] Department of Mechanical Engineering, Faculty of Engineering, Imam Khomeini International University, Qazvin, Iran

[2] School of Mechanical Engineering, College of Engineering, University of Tehran, Tehran, Iran

Published online: 13 April 2021

consideration of the influence of the CNTs' agglomeration on the total stiffness of a polymeric CNTR nanocomposite was introduced in Ref. [39]. Also, in the recent investigation reported in Ref. [40], the viscoelastic nature of the polymer matrix is taken into consideration based upon a theoretical point of view dealing with the inclusion of the influence of the internal characteristics relaxation time of the polymer on the equivalent stiffness of the CNTR polymer.

Besides, a novel type of nanocomposites has been developed which is able to promote much better mechanical properties in comparison with the conventional ones. In this new category of such nanomaterials, macroscale reinforcing agents are used in conjunction with nanoparticles. According to this issue, they are usually called multi-scale hybrid (MSH) nanocomposites. In the recent years, a mentionable portion of the studies about nanocomposite materials and structures was concerned with MSH nanocomposites. For example, the nonlinear dynamic behaviors of MSH nanocomposite plates containing smart piezoelectric fibers were surveyed based on the Mindlin plate theory [41]. In the context of an analytical study, a viscoelastic fractional model was utilized to probe the damped vibrations of the MSH nanocomposite laminates [42]. In this study, the effect of the implementation of either single-walled or multi-walled CNTs (SWCNTs/MWCNTs) on the mechanical performance of the system is illustrated, too. The micromechanical homogenization was adopted in Ref. [43] to analyze the vibrational responses of blades, consisted of MSH nanocomposites, subjected to large deflections. According to a finite element (FE)-assisted framework, the low-velocity impact reaction of the rectangular plates consisted of MSH nanocomposites was monitored whenever the continuous system is subjected to variation in local temperature and moisture concentration [44]. Furthermore, the nonlinear mechanical characteristics of MSH nanocomposite beams manufactured from graphene nanosheets were examined on the basis of theoretical homogenization techniques [45]. The thermal conductivity of the MSH nanocomposites fabricated from different types of nanoparticles was measured on the basis of the well-known thermogravimetric analysis (TGA) [46]. The FE investigation of the free vibration problem of a three-phase MSH nanocomposite beam based on the refined-type beam theorem was accomplished in Ref. [47]. In addition, an analytical approach was organized in Ref. [48] to probe the static buckling characteristics of MSH nanocomposite plates with the aid of the Kirchhoff–Love plate hypothesis. In the above references, the MSH nanocomposite material was modeled on the basis of a simple micromechanical scheme, namely Halpin–Tsai method. However, a group of Iranian researchers utilized a complicated homogenization technique, inspired from the combination of Eshelby and Mori–Tanaka methods, for the goal of considering the influences of the agglomeration of the nanoparticles on the static and dynamic responses of MSH nanocomposite structures [49–56].

Although a wide range of attempts are already made toward analyzing the mechanical behaviors of MSH nanocomposite structures, there exists no article addressing the coupled influences of waviness of CNTs and time-dependent nature of the polymer on the dynamic responses of MSH nanocomposite structures. Therefore, authors were motivated to compensate this lack of data herein with the aid of advanced micromechanical schemes. The Young's modulus of the polymer will be considered as an exponential function of time by the means of characteristic time and stretching power component introduced in [40]. Then, the modified form of the Halpin–Tsai method [38] will be implemented to attain the material properties of the CNTR nanocomposites including wavy CNTs. At the end, the modified form of the rule of the mixture will be hired to derive the material properties of the MSH nanocomposite. Once the aforesaid process is completed, the kinematic relations will be adopted based on the refined higher-order shear deformation theory (HSDT) of plates. Finally, the dynamic form of the virtual work's principle will be employed to derive the governing equations which will be thereafter solved on the basis of the Galerkin's analytical method.

2 Theory and formulation

2.1 Micromechanical homogenization

In this part, the material properties of the MSH nanocomposite, whose schematic composition is illustrated in Fig. 1, will be derived in a hierarchical procedure. First of all, the properties of polymer will be probed. Polymers are well known to exhibit viscoelastic material behavior. Such soft materials are usually characterized by their long-term mechanical behavior due to their viscoelastic nature that they exhibit under mechanical and/or environmental loading

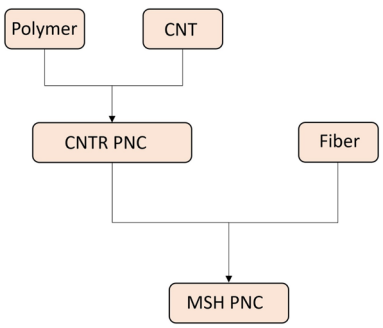

Fig. 1 Schematic illustration of the MSH nanocomposites

[57]. In general, polymers manifest a nonlinear behavior from themselves in the time domain and, therefore, their rheological features must be taken into consideration by the means of regarding for the gradual changes in their compliance (or stiffness) as time exceeds [58]. In this research, the mechanical properties of the polymeric matrix, namely E_{PM} and ν_{PM}, are presumed to be time-dependent with the aid of an exponential function of time. According to the Maxwell model [40, 59], Young's modulus of the polymers can be presented in the following form:

$$E_{PM}(t) = E^0_{PM} \exp\left(-\frac{t}{\tau_v}\right)^{\beta_v}, \tag{1}$$

where E^0_{PM} is the instantaneous elastic modulus at the initial time. The parameters β_v and τ_v are the stretching exponent and characteristic relaxation time, respectively. Similarly, the Poisson's ratio can be presumed to be in the below time-dependent form:

$$\nu_{PM}(t) = 0.5 - (0.5 - \nu^0_{PM}) \exp\left(-\frac{t}{\tau_v}\right)^{\beta_v}, \tag{2}$$

which ν^0_{PM} represents the initial value of the Poisson's ratio. It should be remembered that the polymer's density is not time-dependent; therefore, $\rho^0_{PM} = \rho_{PM}$.

Now, the material properties of the polymer matrix are in hand and it is time to go through finding the effective material properties of the CNTR nanocomposite. To this purpose and with regard to the negative influence of the existence of wavy CNTs on the total stiffness of the nanocomposite material, the modified form of the Halpin–Tsai [38] will be utilized. The aforementioned model can be utilized in the cases that lower than 2% of the nanocomposite's volume is assumed to be consisted of reinforcing CNTs. In the mentioned domain, the results of this model were proven to be in accordance with those achieved from the experiments [38]. Based on this method, the Young's modulus of the CNTR nanocomposite can be written as below [38]:

$$E_{NCM} = \frac{1 + C\eta V_{CNT}}{1 - \eta V_{CNT}} E_{PM}, \tag{3}$$

where

$$\eta = \frac{C_w\left[\alpha E_{CNT}/E_{PM}\right] - 1}{C_w\left[\alpha E_{CNT}/E_{PM}\right] + C}. \tag{4}$$

In Eqs. (3) and (4), the term α is the factor of orientation introduced in Ref. [60]. Also, C is the size-dependent coefficient equal to two times the ratio between the length and the diameter of the CNTs. α is considered equal to $1/6$ because the length of the CNTs is small compared to the total thickness of the structure (i.e., in the range of millimeters) [60]. Besides, C_w is the waviness coefficient and can be varied from zero to one. In fact, this coefficient will define the amplitude of the wave produced by the CNTs' curvature. In other words, if this coefficient is considered to be at its upper limit, all CNTs are straight. The half-circle shape of the CNTs can also be imagined as long as the waviness factor is assumed to be zero. The mass density and Poisson's ratio of the CNTR nanocomposite can be derived using the definition of the rule of the mixture:

$$\rho_{NCM} = \rho_{CNT} V_{CNT} + \rho_{PM} V_{PM}, \tag{5}$$

$$\nu_{NCM} = \nu_{CNT} V_{CNT} + \nu_{PM} V_{PM}. \tag{6}$$

Combining definitions presented in Eqs. (3) and (6), the shear modulus of the CNTR nanocomposite can be presented as below:

$$G_{NCM} = \frac{E_{NCM}}{2\left(1 + \nu_{NCM}\right)}. \tag{7}$$

In Eqs. (3), (5), and (6), the volume fraction of the CNTs in the CNTR nanocomposite can be calculated using the following definition [40]:

$$V_{CNT} = \left(\frac{\rho_{CNT}}{m_r \rho_{PM}} - \frac{\rho_{CNT}}{\rho_{PM}} + 1\right)^{-1}, \tag{8}$$

where ρ_{CNT} and ρ_{PM} are the mass densities of CNTs and polymer matrix, respectively. In addition, m_r is the mass fraction of the reinforcing phase, i.e., CNT.

Now, the material properties of the MSH nanocomposite can be achieved. To this end, the CNTR nanocomposite, whose material properties are presented in Eqs. (3), (5)–(7), must be considered as the matrix of a composite material whose reinforcing agent is glass fiber (GF). The reinforcing fibers are characterized by the corresponding Young's modulus E_F, shear modulus G_F, and Poisson's ratio ν_F. Herein, the fibers are considered to be isotropic solids. The volume fraction of the GFs can be determined using the below expression [40]:

$$V_F = \left(\frac{\rho_F}{m_f \rho_{NCM}} - \frac{\rho_F}{\rho_{NCM}} + 1\right)^{-1}, \tag{9}$$

in which the mass density of fibers is shown with ρ_F and m_f corresponds with the mass fraction of the fibers. The mechanical properties of the MSH nanocomposite can be assessed implementing the rule of the mixture as follows:

$$E_{11} = E_F V_F + E_{NCM} V^*_{PM}, \tag{10}$$

$$E_{22} = E_{33} = \frac{E_{NCM}}{1 - V_F(1 - E_{NCM}/E_F)}, \tag{11}$$

$$G_{12} = G_{13} = G_{23} = \frac{G_{\mathrm{NCM}}}{1 - V_{\mathrm{F}}(1 - G_{\mathrm{NCM}}/G_{\mathrm{F}})}, \tag{12}$$

$$\nu_{12} = \nu_{13} = \nu_{\mathrm{F}} V_{\mathrm{F}} + \nu_{\mathrm{NCM}} V^{*}_{\mathrm{PM}}, \tag{13}$$

$$\nu_{23} = \frac{E_{22}}{2G_{23}} - 1, \tag{14}$$

where E_{11}, E_{22}, and E_{33} denote Young's modulus in the axial, transverse, and flexural directions, respectively. Also, the shear modules in the planes constructed from the intersection of the aforementioned directions are shown with G_{12}, G_{13}, and G_{23}. The Poisson's ratios in the mentioned planes are presented with ν_{12}, ν_{13}, and ν_{23}.

2.2 Refined plate theory

In this section, the kinematic relations needed to derive the components of the strain tensor of the continuous system will be presented. The shear strain and stress profiles are evaluated by a shape function in the HSDTs. In such theories, the distribution of shear strain and stress across the thickness can be approximated in addition to satisfaction of existence of no shear stress at the free edges of the structure [61–63]. According to this type of the plate theories, the displacement field of the structure can be described as below:

$$\begin{aligned}
u_x(x,y,z,t) &= u(x,y,t) - z\frac{\partial w_{\mathrm{b}}(x,y,t)}{\partial x} - f(z)\frac{\partial w_{\mathrm{s}}(x,y,t)}{\partial x},\\
u_y(x,y,z,t) &= v(x,y,t) - z\frac{\partial w_{\mathrm{b}}(x,y,t)}{\partial y} - f(z)\frac{\partial w_{\mathrm{s}}(x,y,t)}{\partial y},\\
u_z(x,y,z,t) &= w_{\mathrm{b}}(x,y,t) + w_{\mathrm{s}}(x,y,t),
\end{aligned} \tag{15}$$

where u and v represent the longitudinal and transverse displacements of the mid-surface, respectively. The deflections caused by bending and shear modes through z-axis are shown with w_{b} and w_{s}, respectively. Also, $f(z)$ stands for the shape function of the theorem. In this study, the shape function is considered to be similar with that introduced in Ref. [64]:

$$f(z) = \frac{h\mathrm{e}^{z}}{h^2 + \pi^2}\left[\pi \sin\left(\frac{\pi z}{h}\right) + h\cos\left(\frac{\pi z}{h}\right)\right] - \frac{h^2}{h^2 + \pi^2}. \tag{16}$$

Now, the components of the nonzero strain tensor of the plate can be written as below:

$$\begin{Bmatrix} \varepsilon_{xx} \\ \varepsilon_{yy} \\ \gamma_{xy} \end{Bmatrix} = \begin{Bmatrix} \varepsilon^{0}_{xx} \\ \varepsilon^{0}_{yy} \\ \gamma^{0}_{xy} \end{Bmatrix} + z\begin{Bmatrix} \kappa^{b}_{xx} \\ \kappa^{b}_{yy} \\ \kappa^{b}_{xy} \end{Bmatrix} + f(z)\begin{Bmatrix} \kappa^{s}_{xx} \\ \kappa^{s}_{yy} \\ \kappa^{s}_{xy} \end{Bmatrix}, \quad \begin{Bmatrix} \gamma_{xz} \\ \gamma_{yz} \end{Bmatrix} = g(z)\begin{Bmatrix} \gamma^{0}_{xz} \\ \gamma^{0}_{yz} \end{Bmatrix}, \tag{17}$$

where

$$\begin{Bmatrix} \varepsilon^{0}_{xx} \\ \varepsilon^{0}_{yy} \\ \gamma^{0}_{xy} \end{Bmatrix} = \begin{Bmatrix} \frac{\partial u}{\partial x} \\ \frac{\partial v}{\partial y} \\ \frac{\partial u}{\partial x} + \frac{\partial v}{\partial y} \end{Bmatrix}, \quad \begin{Bmatrix} \kappa^{b}_{xx} \\ \kappa^{b}_{yy} \\ \kappa^{b}_{xy} \end{Bmatrix} = \begin{Bmatrix} -\frac{\partial^2 w_{\mathrm{b}}}{\partial x^2} \\ -\frac{\partial^2 w_{\mathrm{b}}}{\partial y^2} \\ -2\frac{\partial^2 w_{\mathrm{b}}}{\partial x \partial y} \end{Bmatrix},$$
$$\begin{Bmatrix} \kappa^{s}_{xx} \\ \kappa^{s}_{yy} \\ \kappa^{s}_{xy} \end{Bmatrix} = \begin{Bmatrix} -\frac{\partial^2 w_{\mathrm{s}}}{\partial x^2} \\ -\frac{\partial^2 w_{\mathrm{s}}}{\partial y^2} \\ -2\frac{\partial^2 w_{\mathrm{s}}}{\partial x \partial y} \end{Bmatrix}, \quad \begin{Bmatrix} \gamma^{0}_{xz} \\ \gamma^{0}_{yz} \end{Bmatrix} = \begin{Bmatrix} \frac{\partial w_{\mathrm{s}}}{\partial x} \\ \frac{\partial w_{\mathrm{s}}}{\partial y} \end{Bmatrix}. \tag{18}$$

2.3 Motion equations

The well-known Hamilton's principle will be employed in this section to derive the motion equations of the plate-type element. The mathematical definition of this principle in general form can be written as below [65]:

$$\int_0^t \delta(U - T)\mathrm{d}t = 0, \tag{19}$$

where U and T stand for the strain and kinetic energies, respectively. Now, the variations of each of the aforementioned energies must be determined accordingly. First, the variation of the strain energy can be shown in the following form:

$$\begin{aligned}
\delta U &= \int_V (\sigma_{xx}\delta\varepsilon_{xx} + \sigma_{yy}\delta\varepsilon_{yy} + \sigma_{xy}\delta\gamma_{xy} + \sigma_{xz}\delta\gamma_{xz} + \sigma_{yz}\delta\gamma_{yz})\mathrm{d}V\\
&= \int_0^b \int_0^a \begin{pmatrix} N_{xx}\delta\varepsilon^{0}_{xx} + M^{b}_{xx}\delta\kappa^{b}_{xx} + M^{s}_{xx}\delta\kappa^{s}_{xx} + N_{yy}\delta\varepsilon^{0}_{yy} + \\ M^{b}_{yy}\delta\kappa^{b}_{yy} + M^{s}_{yy}\delta\kappa^{s}_{yy} + N_{xy}\delta\gamma^{0}_{xy} + M^{b}_{xy}\delta\kappa^{b}_{xy} + \\ M^{s}_{xy}\delta\kappa^{s}_{xy} + Q_{xy}\delta\gamma^{0}_{xy} + Q_{yz}\delta\gamma^{0}_{yz} \end{pmatrix}\mathrm{d}x\mathrm{d}y.
\end{aligned} \tag{20}$$

In the above definition, the stress-resultants can be defined in the following form:

$$\begin{aligned}
(N_{ij}, M^{b}_{ij}, M^{s}_{ij}) &= \int_{-h/2}^{h/2} (1, z, f(z))\sigma_{ij}\mathrm{d}z, \quad (i,j = x,y)\\
Q_k &= \int_{-h/2}^{h/2} g(z)\sigma_k \mathrm{d}z, \quad (k = xz, yz),
\end{aligned} \tag{21}$$

in which $g(z) = 1 - df(z)/dz$. Besides, the variation of the kinetic energy of the system can be described in the following form:

$$\delta T = \int_V \left(\frac{\partial u_x}{\partial t}\frac{\partial \delta u_x}{\partial t} + \frac{\partial u_y}{\partial t}\frac{\partial \delta u_y}{\partial t} + \frac{\partial u_z}{\partial t}\frac{\partial \delta u_z}{\partial t} \right) \rho \mathrm{d}V$$

$$= \int_0^b \int_0^a \left(\begin{array}{c} I_0 \left[\frac{\partial u}{\partial t}\frac{\partial \delta u}{\partial t} + \frac{\partial v}{\partial t}\frac{\partial \delta v}{\partial t} + \frac{\partial (w_\mathrm{b}+w_\mathrm{s})}{\partial t}\frac{\partial \delta (w_\mathrm{b}+w_\mathrm{s})}{\partial t} \right] \\ -I_1 \left[\frac{\partial u}{\partial t}\frac{\partial^2 \delta w_\mathrm{b}}{\partial x \partial t} + \frac{\partial^2 w_\mathrm{b}}{\partial x \partial t}\frac{\partial \delta u}{\partial t} + \frac{\partial v}{\partial t}\frac{\partial^2 \delta w_\mathrm{b}}{\partial y \partial t} + \frac{\partial^2 w_\mathrm{b}}{\partial y \partial t}\frac{\partial \delta v}{\partial t} \right] \\ -J_1 \left[\frac{\partial u}{\partial t}\frac{\partial^2 \delta w_\mathrm{s}}{\partial x \partial t} + \frac{\partial^2 w_\mathrm{s}}{\partial x \partial t}\frac{\partial \delta u}{\partial t} + \frac{\partial v}{\partial t}\frac{\partial^2 \delta w_\mathrm{s}}{\partial y \partial t} + \frac{\partial^2 w_\mathrm{s}}{\partial y \partial t}\frac{\partial \delta v}{\partial t} \right] \\ +I_2 \left[\frac{\partial^2 w_\mathrm{b}}{\partial x \partial t}\frac{\partial^2 \delta w_\mathrm{b}}{\partial x \partial t} + \frac{\partial^2 w_\mathrm{b}}{\partial y \partial t}\frac{\partial^2 \delta w_\mathrm{b}}{\partial y \partial t} \right] + K_2 \left[\frac{\partial^2 w_\mathrm{s}}{\partial x \partial t}\frac{\partial^2 \delta w_\mathrm{s}}{\partial x \partial t} + \frac{\partial^2 w_\mathrm{s}}{\partial y \partial t}\frac{\partial^2 \delta w_\mathrm{s}}{\partial y \partial t} \right] \\ +J_2 \left[\frac{\partial^2 w_\mathrm{b}}{\partial x \partial t}\frac{\partial^2 \delta w_\mathrm{s}}{\partial x \partial t} + \frac{\partial^2 w_\mathrm{s}}{\partial x \partial t}\frac{\partial^2 \delta w_\mathrm{b}}{\partial x \partial t} + \frac{\partial^2 w_\mathrm{b}}{\partial y \partial t}\frac{\partial^2 \delta w_\mathrm{s}}{\partial y \partial t} + \frac{\partial^2 w_\mathrm{s}}{\partial y \partial t}\frac{\partial^2 \delta w_\mathrm{b}}{\partial y \partial t} \right] \end{array} \right) \mathrm{d}x\mathrm{d}y. \tag{22}$$

In the above relation, the through-the-thickness mass moments of inertia can be calculated using the following definitions:

$$[I_0, I_1, J_1, I_2, J_2, K_2] = \int_{-h/2}^{h/2} [1, z, f(z), z^2, zf(z), f^2(z)] \rho \mathrm{d}z. \tag{23}$$

By setting the coefficient of δu, δv, δw_b, and δw_s to zero, the Euler–Lagrange equations of the MSH nanocomposite plate can be obtained by substituting for the variations of the strain and kinetic energies from Eqs. (20) and (22), respectively, into Eq. (19):

$$\frac{\partial N_{xx}}{\partial x} + \frac{\partial N_{xy}}{\partial y} = I_0 \frac{\partial^2 u}{\partial t^2} - I_1 \frac{\partial^3 w_\mathrm{b}}{\partial x \partial t^2} - J_1 \frac{\partial^3 w_\mathrm{s}}{\partial x \partial t^2}, \tag{24}$$

$$\frac{\partial N_{xy}}{\partial x} + \frac{\partial N_{yy}}{\partial y} = I_0 \frac{\partial^2 v}{\partial t^2} - I_1 \frac{\partial^3 w_\mathrm{b}}{\partial y \partial t^2} - J_1 \frac{\partial^3 w_\mathrm{s}}{\partial y \partial t^2}, \tag{25}$$

$$\frac{\partial^2 M^b_{xx}}{\partial x^2} + 2\frac{\partial^2 M^b_{xy}}{\partial x \partial y} + \frac{\partial^2 M^b_{yy}}{\partial^2 y} = I_0 \frac{\partial^2 (w_\mathrm{b}+w_\mathrm{s})}{\partial t^2} + I_1 \left(\frac{\partial^3 u}{\partial x \partial t^2} + \frac{\partial^3 v}{\partial y \partial t^2} \right) - I_2 \left(\frac{\partial^4 w_\mathrm{b}}{\partial t^2 \partial x^2} + \frac{\partial^4 w_\mathrm{b}}{\partial y^2 \partial x^2} \right) - J_2 \left(\frac{\partial^4 w_\mathrm{s}}{\partial x^2 \partial t^2} + \frac{\partial^4 w_\mathrm{s}}{\partial y^2 \partial t^2} \right), \tag{26}$$

$$\frac{\partial^2 M^s_{xx}}{\partial x^2} + 2\frac{\partial^2 M^s_{xy}}{\partial x \partial y} + \frac{\partial^2 M^s_{yy}}{\partial^2 y} + \frac{\partial Q_{xz}}{\partial x} + \frac{\partial Q_{yz}}{\partial y} = I_0 \frac{\partial^2 (w_\mathrm{b}+w_\mathrm{s})}{\partial t^2} + J_1 \left(\frac{\partial^3 u}{\partial x \partial t^2} + \frac{\partial^3 v}{\partial y \partial t^2} \right) - J_2 \left(\frac{\partial^4 w_\mathrm{b}}{\partial x^2 \partial t^2} + \frac{\partial^4 w_\mathrm{b}}{\partial y^2 \partial x^2} \right) - K_2 \left(\frac{\partial^4 w_\mathrm{s}}{\partial x^2 \partial t^2} + \frac{\partial^4 w_\mathrm{s}}{\partial y^2 \partial t^2} \right). \tag{27}$$

Integration by parts gives the following classical boundary conditions (BCs) at edges $x = 0$ or a and $y = 0$ or b as follows:

$$\begin{array}{l} \text{Specify } w_\mathrm{b} \text{ or } \left(\frac{\partial M^b_{xx}}{\partial x} + \frac{\partial M^b_{xy}}{\partial y} \right) n_x + \left(\frac{\partial M^b_{xy}}{\partial x} + \frac{\partial M^b_{yy}}{\partial y} \right) n_y = 0, \\ \text{Specify } w_\mathrm{s} \text{ or } \left(\frac{\partial M^s_{xx}}{\partial x} + \frac{\partial M^s_{xy}}{\partial y} + Q_{xz} \right) n_x + \left(\frac{\partial M^s_{xy}}{\partial x} + \frac{\partial M^s_{yy}}{\partial y} + Q_{yz} \right) n_y = 0, \\ \text{Specify } \frac{\partial w_\mathrm{b}}{\partial n} \text{ or } M^b_{xx} n_x^2 + M^b_{xy} n_x n_y + M^b_{yy} n_y^2 = 0. \end{array} \tag{28}$$

in which $\frac{\partial (.)}{\partial n} = \frac{\partial (.)}{\partial x} n_x + \frac{\partial (.)}{\partial y} n_y$. It is worth mentioning that the longitudinal and transverse components of the unit vector normal on the boundary of the structure are shown with n_x and n_y, respectively. In addition, the non-classical BCs can be expressed in the following form:

$$\text{Specify } \frac{\partial^2 w_b}{\partial x^2} = 0, \quad \text{Specify } \frac{\partial^2 w_b}{\partial y^2} = 0,$$
$$\text{Specify } \frac{\partial^2 w_s}{\partial x^2} = 0, \quad \text{Specify } \frac{\partial^2 w_s}{\partial y^2} = 0. \tag{29}$$

2.4 Constitutive equations

In this part, elastic stress–strain relations of the nanocomposite material are depicted. According to the constitutive relations of linearly solids, the stress and strain tensors can be related to each other using the following definition:

$$\sigma_{ij} = C_{ijkl}\varepsilon_{kl}, \tag{30}$$

in which σ_{ij} and ε_{kl} are the components of the second-order stress and strain tensors, respectively. Also, C_{ijkl} represents the component of the fourth-order elasticity tensor. By considering the plane-stress assumption, the below relation between stress and strain can be achieved:

$$\begin{bmatrix} \sigma_{xx} \\ \sigma_{yy} \\ \sigma_{yz} \\ \sigma_{xz} \\ \sigma_{xy} \end{bmatrix} = \begin{bmatrix} Q_{11} & Q_{12} & 0 & 0 & 0 \\ Q_{12} & Q_{22} & 0 & 0 & 0 \\ 0 & 0 & Q_{44} & 0 & 0 \\ 0 & 0 & 0 & Q_{55} & 0 \\ 0 & 0 & 0 & 0 & Q_{66} \end{bmatrix} \begin{bmatrix} \varepsilon_{xx} \\ \varepsilon_{yy} \\ \varepsilon_{yz} \\ \varepsilon_{xz} \\ \varepsilon_{xy} \end{bmatrix}, \tag{31}$$

where,

$$Q_{11} = \frac{E_{11}}{1-\nu_{12}\nu_{21}}, \; Q_{12} = \frac{\nu_{12}E_{22}}{1-\nu_{12}\nu_{21}}, \; Q_{22} = \frac{E_{22}}{1-\nu_{12}\nu_{21}},$$
$$Q_{44} = G_{23}, \quad Q_{55} = G_{13}, \quad Q_{66} = G_{12}. \tag{32}$$

Once Eq. (31) is integrated over the thickness of the plate with regard to the definitions of the stress resultants previously mentioned in Eq. (18), the below relations between the stress resultants and displacement field of the nanocomposite plate can be achieved:

$$\begin{bmatrix} N_{xx} \\ N_{yy} \\ N_{xy} \\ M^b_{xx} \\ M^b_{yy} \\ M^b_{xy} \\ M^s_{xx} \\ M^s_{yy} \\ M^s_{xy} \end{bmatrix} = \begin{bmatrix} A_{11} & A_{12} & 0 & B_{11} & B_{12} & 0 & B^s_{11} & B^s_{12} & 0 \\ A_{12} & A_{22} & 0 & B_{12} & B_{22} & 0 & B^s_{12} & B^s_{22} & 0 \\ 0 & 0 & A_{66} & 0 & 0 & B_{66} & 0 & 0 & B^s_{66} \\ B_{11} & B_{12} & 0 & D_{11} & D_{12} & 0 & D^s_{11} & D^s_{12} & 0 \\ B_{12} & B_{22} & 0 & D_{12} & D_{22} & 0 & D^s_{12} & D^s_{22} & 0 \\ 0 & 0 & B_{66} & 0 & 0 & D_{66} & 0 & 0 & D^s_{66} \\ B^s_{11} & B^s_{12} & 0 & D^s_{11} & D^s_{12} & 0 & H^s_{11} & H^s_{12} & 0 \\ B^s_{12} & B^s_{22} & 0 & D^s_{12} & D^s_{22} & 0 & H^s_{12} & H^s_{22} & 0 \\ 0 & 0 & B^s_{66} & 0 & 0 & D^s_{66} & 0 & 0 & H^s_{66} \end{bmatrix} \begin{bmatrix} \frac{\partial u}{\partial x} \\ \frac{\partial v}{\partial y} \\ \frac{\partial u}{\partial x} + \frac{\partial v}{\partial y} \\ -\frac{\partial^2 w_b}{\partial x^2} \\ -\frac{\partial^2 w_b}{\partial y^2} \\ -2\frac{\partial^2 w_b}{\partial x \partial y} \\ -\frac{\partial^2 w_s}{\partial x^2} \\ -\frac{\partial^2 w_s}{\partial y^2} \\ -\frac{\partial^2 w_s}{\partial x^2} \end{bmatrix},$$
$$\begin{bmatrix} Q_{xz} \\ Q_{yz} \end{bmatrix} = \begin{bmatrix} A^s_{44} & 0 \\ 0 & A^s_{55} \end{bmatrix} \begin{bmatrix} \frac{\partial w_s}{\partial x} \\ \frac{\partial w}{\partial y} \end{bmatrix} \tag{33}$$

The through-the-thickness rigidities used in the above relations can be computed using the below definitions:

$$[A_n, B_n, B^s_n, D_n, D^s_n, H^s_n] = \int_{-h/2}^{h/2} [1, z, f(z), z^2, zf(z), f^2(z)] Q_n(z) \mathrm{d}z,$$
$$n = (11, 12, 22, 66)[A^s_{44}, A^s_{55}] = \int_{-h/2}^{h/2} [Q_{44}(z),\ Q_{55}(z)] g^2(z) \mathrm{d}z. \tag{34}$$

2.5 Governing equations

In this part, the mathematical formulation of the problem will be completed by substituting for the stress resultants from Eq. (33) into the Euler–Lagrange equations formerly presented in Eqs. (24)–(27). Once the above substitution is accomplished, the governing equations of the nanocomposite plate can be presented in the below form:

$$A_{11}\frac{\partial^2 u}{\partial x^2} + A_{66}\frac{\partial^2 u}{\partial y^2} + (A_{12}+A_{66})\frac{\partial^2 v}{\partial x \partial y} - B_{11}\frac{\partial^3 w_b}{\partial x^3} - (B_{12}+2B_{66})\frac{\partial^3 w_b}{\partial x \partial y^2}$$
$$- B^s_{11}\frac{\partial^3 w_s}{\partial x^3} - (B^s_{12}+2B^s_{66})\frac{\partial^3 w_s}{\partial x \partial y^2} - I_0\frac{\partial^2 u}{\partial t^2} + I_1\frac{\partial^3 w_b}{\partial x \partial t^2} + J_1\frac{\partial^3 w_s}{\partial x \partial t^2} = 0, \tag{35}$$

$$(A_{12}+A_{66})\frac{\partial^2 u}{\partial x \partial y} + A_{66}\frac{\partial^2 v}{\partial x^2} + A_{22}\frac{\partial^2 v}{\partial y^2} - (B_{12}+2B_{66})\frac{\partial^3 w_b}{\partial x^2 \partial y} - B_{22}\frac{\partial^3 w_b}{\partial y^3}$$
$$- (B^s_{12}+2B^s_{66})\frac{\partial^3 w_s}{\partial x^2 \partial y} - B^s_{22}\frac{\partial^3 w_s}{\partial y^3} - I_0\frac{\partial^2 v}{\partial t^2} + I_1\frac{\partial^3 w_b}{\partial y \partial t^2} + J_1\frac{\partial^3 w_s}{\partial y \partial t^2} = 0, \tag{36}$$

Table 1 Material properties of polymer matrix, glass fiber, and CNT

Material properties of polymer [40]
$E_{PM}^{0} = 2.1$ GPa, $\nu_{PM}^{0} = 0.34$, and $\rho_{PM} = 1150$ kg/m^3
Material properties of glass fiber [40]
$E_F = 71$ GPa, $G_F = 30$ GPa, $\nu_F = 0.22$, and $\rho_F = 2450$ kg/m^3
Material properties of carbon nanotube [44]
$E_{CNT} = 640(1 - 0.0005\Delta T)$ GPa, $\nu_{CNT} = 0.33$, $\rho_{CNT} = 1350$ kg/m^3, $l_{CNT} = 25\ \mu m$, and $d_{CNT} = 1.4$ nm

$$
\begin{aligned}
&B_{11}\frac{\partial^3 u}{\partial x^3} + (B_{12} + 2B_{66})\left(\frac{\partial^3 u}{\partial x \partial y^2} + \frac{\partial^3 v}{\partial x^2 \partial y}\right) + B_{22}\frac{\partial^3 v}{\partial y^3} \\
&\quad - D_{11}\frac{\partial^4 w_b}{\partial x^4} - 2(D_{12} + 2D_{66})\frac{\partial^4 w_b}{\partial x^2 \partial y^2} \\
&\quad - D_{22}\frac{\partial^4 w_b}{\partial y^4} - D_{11}^{s}\frac{\partial^4 w_s}{\partial x^4} - 2(D_{12}^{s} + 2D_{66}^{s})\frac{\partial^3 w_s}{\partial x^2 \partial y^2} \\
&\quad - D_{22}^{s}\frac{\partial^4 w_s}{\partial y^4} - I_0\frac{\partial^2 (w_b + w_s)}{\partial t^2} - I_1\left(\frac{\partial^3 u}{\partial x \partial t^2} + \frac{\partial^3 v}{\partial y \partial t^2}\right) \\
&\quad + I_2\left(\frac{\partial^4 w_b}{\partial t^2 \partial x^2} + \frac{\partial^4 w_b}{\partial y^2 \partial x^2}\right) + J_2\left(\frac{\partial^4 w_s}{\partial x^2 \partial t^2} + \frac{\partial^4 w_s}{\partial y^2 \partial t^2}\right) = 0,
\end{aligned}
\tag{37}
$$

$$
\begin{aligned}
&B_{11}^{s}\frac{\partial^3 u}{\partial x^3} + (B_{12}^{s} + 2B_{66}^{s})\left(\frac{\partial^3 u}{\partial x \partial y^2} + \frac{\partial^3 v}{\partial x^2 \partial y}\right) + B_{22}^{s}\frac{\partial^3 v}{\partial y^3} \\
&\quad - D_{11}^{s}\frac{\partial^4 w_b}{\partial x^4} - 2(D_{12}^{s} + 2D_{66}^{s})\frac{\partial^4 w_b}{\partial x^2 \partial y^2} \\
&\quad - D_{22}^{s}\frac{\partial^4 w_b}{\partial y^4} - H_{11}^{s}\frac{\partial^4 w_s}{\partial x^4} - 2(H_{12}^{s} + 2H_{66}^{s})\frac{\partial^3 w_s}{\partial x^2 \partial y^2} \\
&\quad - H_{22}^{s}\frac{\partial^4 w_s}{\partial y^4} + A_{55}^{s}\frac{\partial^2 w_s}{\partial x^2} + A_{44}^{s}\frac{\partial^2 w_s}{\partial y^2} \\
&\quad - I_0\frac{\partial^2 (w_b + w_s)}{\partial t^2} - J_1\left(\frac{\partial^3 u}{\partial x \partial t^2} + \frac{\partial^3 v}{\partial y \partial t^2}\right) \\
&\quad + J_2\left(\frac{\partial^4 w_b}{\partial x^2 \partial t^2} + \frac{\partial^4 w_b}{\partial y^2 \partial x^2}\right)) + K_2\left(\frac{\partial^4 w_s}{\partial x^2 \partial t^2} + \frac{\partial^4 w_s}{\partial y^2 \partial t^2}\right) = 0.
\end{aligned}
\tag{38}
$$

3 Analytical solution

There exist a wide range of analytical and numerical methods known by now to analyze the static and dynamic behaviors of continuous systems consisted of either homogeneous or heterogeneous materials [66–92]. Herein, based on Navier method, an analytical solution of the governing equations for free vibration of a simply-supported nanocomposite plate is presented. Therefore, the following expansions of displacements have been assumed:

$$
\begin{aligned}
u &= \sum_{m=1}^{\infty}\sum_{n=1}^{\infty} U_{mn}\cos(\alpha x)\sin(\beta y)e^{i\omega_{mn}t}, \\
v &= \sum_{m=1}^{\infty}\sum_{n=1}^{\infty} V_{mn}\sin(\alpha x)\cos(\beta y)e^{i\omega_{mn}t}, \\
w_b &= \sum_{m=1}^{\infty}\sum_{n=1}^{\infty} W_{bmn}\sin(\alpha x)\sin(\beta y)e^{i\omega_{mn}t}, \\
w_s &= \sum_{m=1}^{\infty}\sum_{n=1}^{\infty} W_{smn}\sin(\alpha x)\sin(\beta y)e^{i\omega_{mn}t},
\end{aligned}
\tag{39}
$$

in which U_{mn}, V_{mn}, W_{bmn}, and W_{smn} are unknown Fourier coefficients. Also, we have $\alpha = \frac{m\pi}{a}$ and $\beta = \frac{m\pi}{b}$. In the above solution functions, all edges are assumed to be simply supported. Hence, below constraints must be considered:

$$
\begin{aligned}
&u = w_b = w_s = N_x = M_x^b = M_x^s = 0 \quad \text{on edge } x = 0, a \\
&u = w_b = w_s = N_y = M_y^b = M_y^s = 0 \quad \text{on edge } y = 0, b.
\end{aligned}
\tag{40}
$$

Here, by inserting Eq. (39) into Eqs. (35)–(38), the matrices resulting by solving the governing equations by Navier solution are given as:

$$
\left\{\mathbf{K} - \omega_{mn}^2\mathbf{M}\right\}\begin{Bmatrix} U_{mn} \\ V_{mn} \\ W_{bmn} \\ W_{smn} \end{Bmatrix} = 0,
\tag{41}
$$

where $\mathbf{K}$ and $\mathbf{M}$ are symmetric stiffness and mass matrices, respectively. The corresponding arrays of the aforementioned matrices can be calculated in the following form:

Table 2 Comparison of the dimensionless natural frequencies of nanocomposite plates reinforced via GPLs

Distribution type	Ref. [93]	Ref. [94]	Present
Neat epoxy	0.058	0.058	0.057
UD	0.122	0.121	0.118
FG-O	0.102	0.097	0.100
FG-X	0.138	0.141	0.128
FG-Λ	0.112	0.117	0.118

Table 3 Comparison of the dimensionless fundamental frequency of CNTR nanocomposite square plates ($a/h=10$)

Volume fraction of the CNTs, V_{CNT}	Ref. [95]	Present
0.11	0.1357	0.1319
0.14	0.1438	0.1400
0.17	0.1685	0.1638

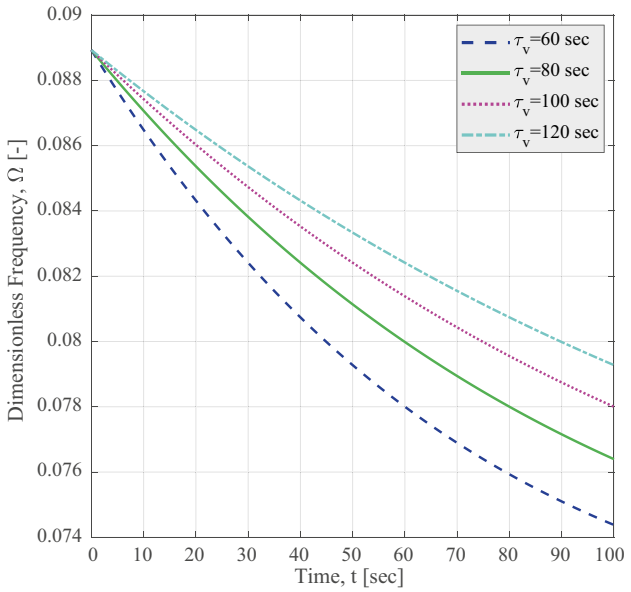

Fig. 2 Variation of the dimensionless frequency of MSH nanocomposite plates versus time once the relaxation time is varied ($m_t=0.2$, $m_r=0.05$, $C_w=0.35$)

$$
\begin{aligned}
&k_{11} = -(A_{11}\alpha^2 + A_{66}\beta^2), \quad k_{12} = -\alpha\beta(A_{12} + A_{66}),\\
&k_{13} = \alpha^3 B_{11} + \alpha\beta^2(B_{12} + 2B_{66}),\\
&k_{14} = B^s_{11}\alpha^3 + \alpha\beta^2(B^s_{12} + 2B^s_{66}),\\
&k_{22} = -(\beta^2 A_{22} + \alpha^2 A_{66}),\\
&k_{23} = \beta^3 B_{22} + \beta\alpha^2(B_{12} + 2B_{66}),\\
&k_{24} = \beta^3 B^s_{22} + \beta\alpha^2(B^s_{12} + 2B^s_{66}),\\
&k_{33} = -(\alpha^4 D_{11} + 2\alpha^2\beta^2(D_{12} + 2D_{66}) + \beta^4 D_{22}),\\
&k_{34} = -(\alpha^4 D^s_{11} + 2\alpha^2\beta^2(D^s_{12} + 2D^s_{12}) + \beta^4 D^s_{22}),\\
&k_{44} = -(\alpha^4 H^s_{11} + 2\alpha^2\beta^2(H^s_{12} + 2H^s_{12})\\
&\qquad + \beta^4 H^s_{22} + \alpha^2 A^s_{44} + \beta^2 A^s_{55}),
\end{aligned}
\tag{42}
$$

and

$$
\begin{aligned}
&m_{11} = I_0, \quad m_{12} = 0, \quad m_{13} = -I_1\alpha, \quad m_{14} = -J_1\alpha, \quad m_{22} = I_0,\\
&m_{23} = -I_1\beta, \quad m_{24} = -J_1\beta, \quad m_{33} = I_0 + I_2(\alpha^2 + \beta^2),\\
&m_{34} = I_0 + J_2(\alpha^2 + \beta^2), \quad m_{44} = I_0 + K_2(\alpha^2 + \beta^2).
\end{aligned}
\tag{43}
$$

4 Numerical results and discussion

This section is presented to discuss about the numerical results of the manuscript. The material properties of the polymer and GF are selected as same as those reported in Ref. [40]. Also, the material properties of the CNTs are gathered from Ref. [44]. The material properties can be simply found in Table 1. In the following illustrations, the thickness of the plate is assumed to be $h = 2$ mm and the length-to-thickness ratio is fixed on $a/h = 10$, unless another value is reported, for the sake of considering the mechanical characteristics of thick-type structures. Moreover, the stretching component is fixed on $\beta_v = 1$ in the numerical results if another value is not reported. On the other hand, the relaxation time is fixed on $\tau_v = 120$ s unless another value is mentioned. In addition, the following dimensionless form of the natural frequency will be used in this study:

$$\Omega = \omega h \sqrt{\frac{\rho^0_{PM}}{E^0_{PM}}}. \tag{44}$$

4.1 Validation study

To show the validity of the provided material, present subsection is devoted to the validity check. To do so, the natural frequencies of the polymer nanocomposite plates reinforced with GPLs were compared with the results reported in Refs. [93] and [94]. According to Table 2, it can be claimed that the results of present study are accurate. It is clear that the differences between the results of ours and aforementioned Refs. are small enough to be dismissed. It is noteworthy that the available small differences are attributed to the difference between the kinematic theories implemented in this research and those utilized in the cited Refs. In addition, the dimensionless frequencies of CNTR plates reported in Ref. [95] are regenerated with an acceptable precision and the results are tabulated in Table 3. According to this secondary validity check, it can be proven that the present methodology is powerful enough to be trusted as a consistent framework for the approximation of the dynamic behaviors of nanocomposite plates.

4.2 Effect of relaxation time on the natural frequency

Figure 2 is depicted to illustrate the variation of the fundamental natural frequency of the MSH nanocomposite plate against time whenever the characteristics time is changed. As shown in the figure, the decreasing trend of the natural

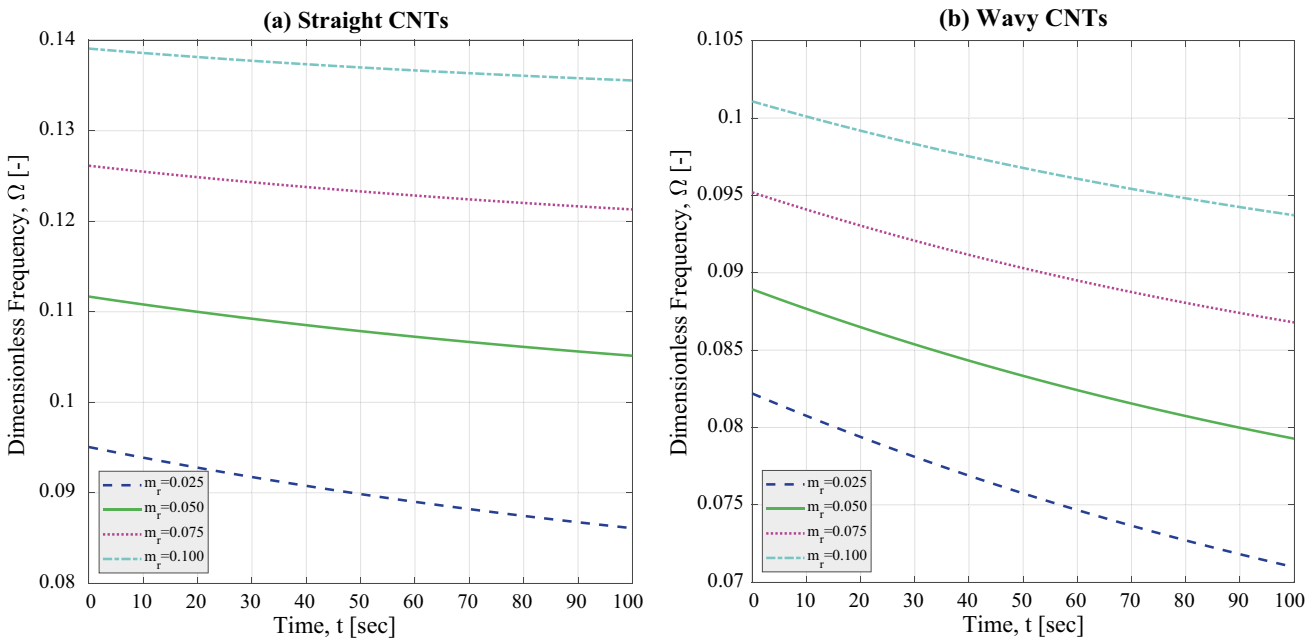

Fig. 3 Variation of the dimensionless frequency of MSH nanocomposite plates containing **a** straight and **b** wavy CNTs versus time once the mass fraction of the CNTs is varied ($m_f = 0.2$)

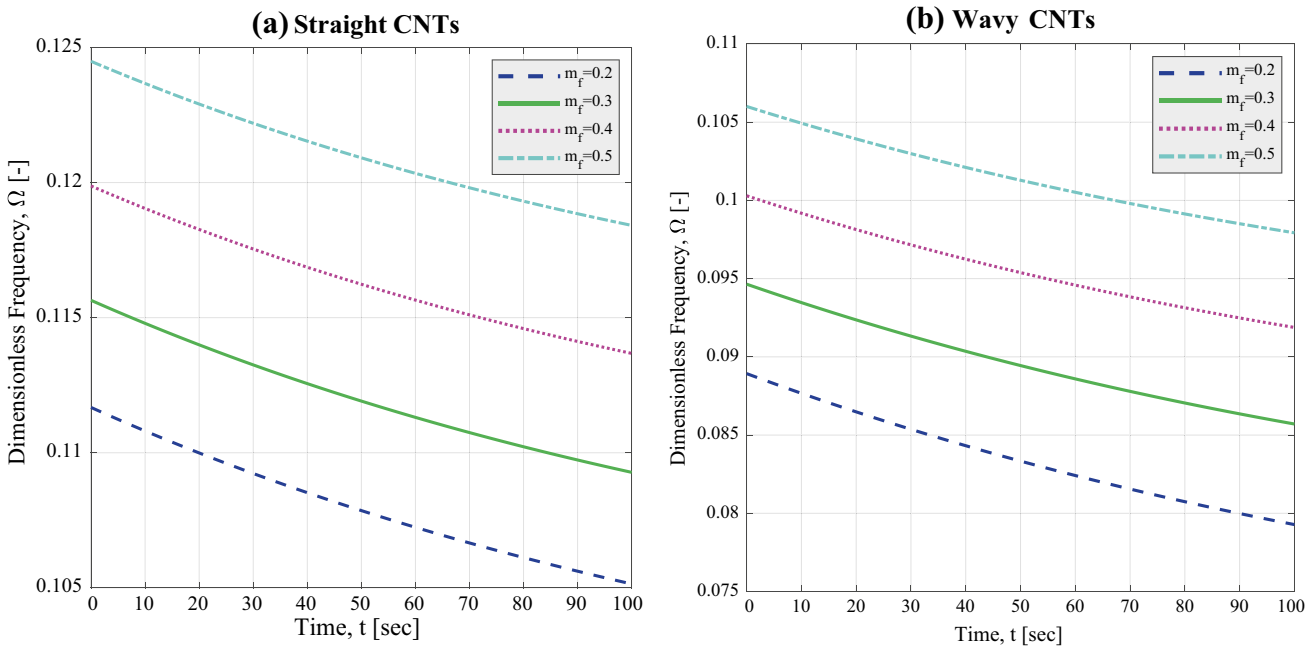

Fig. 4 Variation of the dimensionless frequency of MSH nanocomposite plates containing **a** straight and **b** wavy CNTs versus time once the mass fraction of the GFs is varied ($m_r = 0.05$)

frequency will be postponed by increasing the relaxation time of the polymer matrix. This phenomenon can be justified by recalling the fact that increment of the relaxation time results in the generation of a delay in the attenuation of the polymer's stiffness. Hence, it is natural to observe such a retardation in the time–frequency curve of the plate.

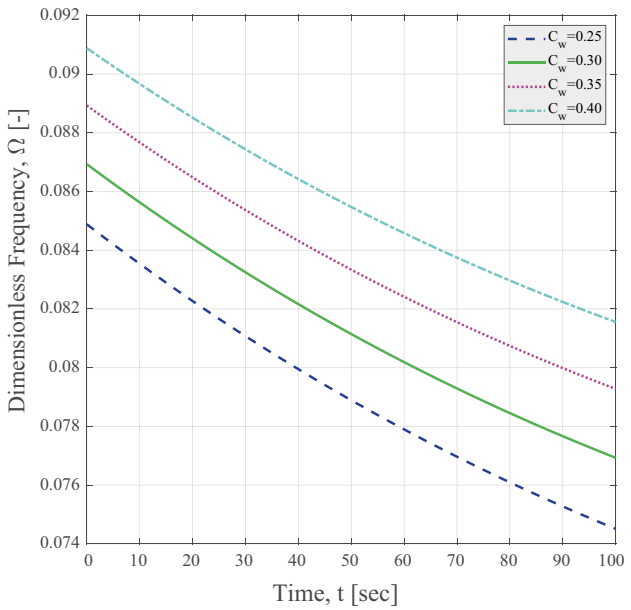

Fig. 5 Variation of the dimensionless frequency of MSH nanocomposite plates versus time once the waviness coefficient is varied (m_r=0.05, m_f=0.2)

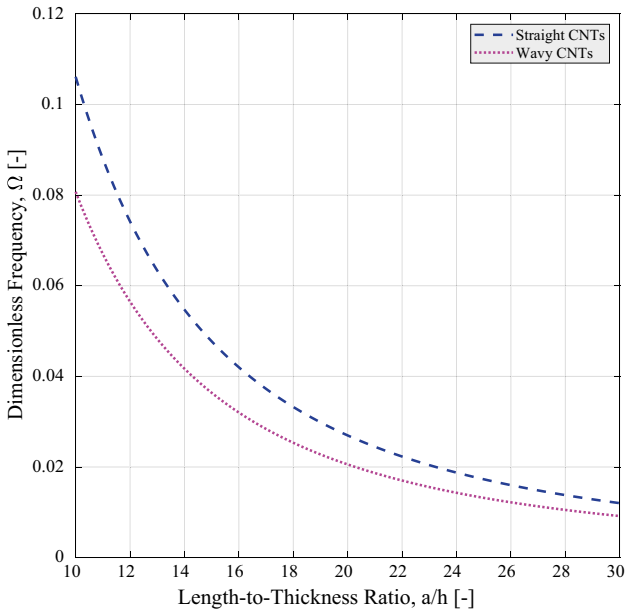

Fig. 6 Variation of the dimensionless frequency of MSH nanocomposite plates versus length-to-thickness ratio for nanocomposite structures reinforced with both straight and wavy CNTs (m_f=0.2, m_r=0.05)

4.3 Effects of the waviness and mass fraction of the CNTs on the natural frequency

The time–frequency curve of the three-phase hybrid nanocomposite structures for various amounts of the mass fraction of either straight or wavy CNTs is presented in Fig. 3. According to this figure, it can be realized that the waviness phenomenon can affect the time–frequency curve of the system in a remarkable manner. Indeed, existence of a wave in the shape of the CNTs results in the reduction of the reinforcing efficiency of the CNTs which leads to the decrease of the total stiffness of the MSH nanocomposite structure. Due to this fact, the natural frequency will be reduced. On the other hand, Fig. 3 reveals that the time–frequency curve can be shifted upward by making a tiny increase in the mass fraction of the CNTs thanks to the exceptional stiffness of the CNTs which can cause noticeable enhancement in the system's dynamic response once the CNT loading in the composition of the hybrid nanomaterial is aggrandized by only a limited value.

4.4 Effects of the CNTs' waviness and GFs' mass fraction on the natural frequency

Similar to Fig. 3, Fig. 4 aims at investigating the impact of changing the mass fraction of the GFs on the time–frequency curve of the MSH nanocomposite plates. It can be perceived that the same trends are valid in this case, too. The reason is of course the positive influence of the reinforcing GFs on the entire stiffness of the three-phase nanomaterial. Actually, the Young's modulus of the GFs is many times greater than that of the polymer matrix and this difference results in such a phenomenon. Once again, it is illustrated that nanocomposite structures consisted of wavy CNTs can provide smaller natural frequencies due to the negative effect of the waviness phenomenon on the stiffness of the nanocomposite.

4.5 Effect of the waviness coefficient on the natural frequency

Another example is shown in Fig. 5 indicating on the impact of the selection of the waviness coefficient on the approximation of the natural frequency of the system. Based on this figure, an enhancement in the value of the waviness coefficient results in a reciprocal improvement in the time–frequency curve in each of the natural modes. The reason is that increasing the waviness coefficient is

corresponding with the consideration of straighter CNTs in the composition of the nanocomposite structure. So, it is not strange to see such an increasing trend because utilization of straight CNTs can be resulted in stiffer nanocomposites. According to the experiments [38], implementation of waviness coefficients in the $0.3 < C_w < 0.4$ range can be resulted into obtaining results in agreement with those observed in the practical cases.

4.6 Effect of length-to-thickness ratio on the natural frequency

As the final case study, Fig. 6 plots the variation of the dimensionless frequency versus length-to-thickness ratio of the plate for the MSH nanocomposite plates reinforced with ideal and non-ideal CNTs. Based on the illustration, it can be perceived that an increase in the length-to-thickness ratio of the plate leads to a reduction in the dimensionless frequency of the plate. With regard to the inverse relation between dimensionless frequency introduced in Eq. (44) and length-to-thickness ratio of the plate, it is natural to observe such a decreasing trend. In any desired length-to-thickness ratio, hybrid nanoengineered plates reinforced with straight CNTs support greater frequencies in comparison with those containing wavy nanotubes. This is due to the destroying impact of the waviness phenomenon on the stiffness of the constituent nanomaterial. It is worth regarding that this prediction can be trusted thanks to the shape function presented in Eq. (16). This function makes it possible to analyze both thin and thick plates accurately; whereas, only thin-walled ones can be studied by classical theory of plates.

5 Conclusions

Present paper was arranged for the purpose of analyzing the mechanical behaviors of three-phase polymer-GF-CNT nanocomposites with respect to the wavy shape of the CNTs and viscoelastic nature of the polymer for the first time. The equivalent material properties were attained in the context of a tri-level hierarchical procedure. Afterward, the governing equations were extracted with the aid of the combination of the refined HSDT and dynamic form of the principle of virtual work. The natural frequencies were derived by the means of the Navier's analytical solution. Now, the most crucial highlights of this study will be reviewed again:

- Implementation of the waviness coefficient of $C_w = 0.35$ provides results close to those reported in the experimental examinations. This selection results in a reliable consideration of the waviness phenomenon.
- An increase in the relaxation time leads to observe higher natural frequencies. Hence, it is recommended to utilize low relaxation times in the theoretical simulations to avoid from engineering overestimations.
- Once the wavy shape of the CNTs and the viscoelastic nature of the polymer matrix are dismissed, the natural frequencies of the system's free vibrations are many times higher than those happening in the practical applications. Therefore, the dynamic stability margin of the nanocomposite system cannot be determined thoroughly.

References

1. Iijima S (1991) Helical microtubules of graphitic carbon. Nature 354(6348):56–58. https://doi.org/10.1038/354056a0
2. Ruoff RS, Lorents DC (1995) Mechanical and thermal properties of carbon nanotubes. Carbon 33(7):925–930. https://doi.org/10.1016/0008-6223(95)00021-5
3. Xie S, Li W, Pan Z, Chang B, Sun L (2000) Mechanical and physical properties on carbon nanotube. J Phys Chem Solids 61(7):1153–1158. https://doi.org/10.1016/S0022-3697(99)00376-5
4. Ajayan PM, Stephan O, Colliex C, Trauth D (1994) Aligned carbon nanotube arrays formed by cutting a polymer resin–nanotube composite. Science 265(5176):1212–1214. https://doi.org/10.1126/science.265.5176.1212
5. Shen H-S, Zhang C-L (2010) Thermal buckling and postbuckling behavior of functionally graded carbon nanotube-reinforced composite plates. Mater Des 31(7):3403–3411. https://doi.org/10.1016/j.matdes.2010.01.048
6. Shen H-S (2011) Postbuckling of nanotube-reinforced composite cylindrical shells in thermal environments, Part II: pressure-loaded shells. Compos Struct 93(10):2496–2503. https://doi.org/10.1016/j.compstruct.2011.04.005
7. Wang Z-X, Shen H-S (2011) Nonlinear vibration of nanotube-reinforced composite plates in thermal environments. Comput Mater Sci 50(8):2319–2330. https://doi.org/10.1016/j.commatsci.2011.03.005
8. Shen H-S, Xiang Y (2012) Nonlinear vibration of nanotube-reinforced composite cylindrical shells in thermal environments. Comput Methods Appl Mech Eng 213–216:196–205. https://doi.org/10.1016/j.cma.2011.11.025
9. Wang Z-X, Shen H-S (2012) Nonlinear dynamic response of nanotube-reinforced composite plates resting on elastic foundations in thermal environments. Nonlinear Dyn 70(1):735–754. https://doi.org/10.1007/s11071-012-0491-2
10. Zhu P, Lei ZX, Liew KM (2012) Static and free vibration analyses of carbon nanotube-reinforced composite plates using finite element method with first order shear deformation plate theory. Compos Struct 94(4):1450–1460. https://doi.org/10.1016/j.compstruct.2011.11.010
11. Lei ZX, Liew KM, Yu JL (2013) Large deflection analysis of functionally graded carbon nanotube-reinforced composite plates by the element-free kp-Ritz method. Comput Methods Appl Mech Eng 256:189–199. https://doi.org/10.1016/j.cma.2012.12.007
12. Rafiee M, Yang J, Kitipornchai S (2013) Thermal bifurcation buckling of piezoelectric carbon nanotube reinforced composite beams. Comput Math Appl 66(7):1147–1160. https://doi.org/10.1016/j.camwa.2013.04.031

13. Rafiee M, Yang J, Kitipornchai S (2013) Large amplitude vibration of carbon nanotube reinforced functionally graded composite beams with piezoelectric layers. Compos Struct 96:716–725. https://doi.org/10.1016/j.compstruct.2012.10.005
14. Ansari R, Faghih Shojaei M, Mohammadi V, Gholami R, Sadeghi F (2014) Nonlinear forced vibration analysis of functionally graded carbon nanotube-reinforced composite Timoshenko beams. Compos Struct 113:316–327. https://doi.org/10.1016/j.compstruct.2014.03.015
15. Rafiee M, He XQ, Liew KM (2014) Non-linear dynamic stability of piezoelectric functionally graded carbon nanotube-reinforced composite plates with initial geometric imperfection. Int J Non-Linear Mech 59:37–51. https://doi.org/10.1016/j.ijnonlinmec.2013.10.011
16. Shen H-S, Xiang Y (2014) Postbuckling of axially compressed nanotube-reinforced composite cylindrical panels resting on elastic foundations in thermal environments. Compos B Eng 67:50–61. https://doi.org/10.1016/j.compositesb.2014.06.020
17. Shen H-S, Xiang Y (2014) Nonlinear vibration of nanotube-reinforced composite cylindrical panels resting on elastic foundations in thermal environments. Compos Struct 111:291–300. https://doi.org/10.1016/j.compstruct.2014.01.010
18. Zhang LW, Song ZG, Liew KM (2015) Nonlinear bending analysis of FG-CNT reinforced composite thick plates resting on Pasternak foundations using the element-free IMLS-Ritz method. Compos Struct 128:165–175. https://doi.org/10.1016/j.compstruct.2015.03.011
19. Duc ND, Cong PH, Tuan ND, Tran P, Thanh NV (2017) Thermal and mechanical stability of functionally graded carbon nanotubes (FG CNT)-reinforced composite truncated conical shells surrounded by the elastic foundations. Thin-Walled Struct 115:300–310. https://doi.org/10.1016/j.tws.2017.02.016
20. Duc ND, Lee J, Nguyen-Thoi T, Thang PT (2017) Static response and free vibration of functionally graded carbon nanotube-reinforced composite rectangular plates resting on Winkler–Pasternak elastic foundations. Aerosp Sci Technol 68:391–402. https://doi.org/10.1016/j.ast.2017.05.032
21. Ebrahimi F, Farazmandnia N (2017) Thermo-mechanical vibration analysis of sandwich beams with functionally graded carbon nanotube-reinforced composite face sheets based on a higher-order shear deformation beam theory. Mech Adv Mater Struct 24(10):820–829. https://doi.org/10.1080/15376494.2016.1196786
22. Memar Ardestani M, Zhang LW, Liew KM (2017) Isogeometric analysis of the effect of CNT orientation on the static and vibration behaviors of CNT-reinforced skew composite plates. Comput Methods Appl Mech Eng 317:341–379. https://doi.org/10.1016/j.cma.2016.12.009
23. Civalek Ö, Baltacıoğlu AK (2018) Vibration of carbon nanotube reinforced composite (CNTRC) annular sector plates by discrete singular convolution method. Compos Struct 203:458–465. https://doi.org/10.1016/j.compstruct.2018.07.037
24. Kiani Y, Mirzaei M (2018) Rectangular and skew shear buckling of FG-CNT reinforced composite skew plates using Ritz method. Aerosp Sci Technol 77:388–398. https://doi.org/10.1016/j.ast.2018.03.022
25. Moradi-Dastjerdi R, Aghadavoudi F (2018) Static analysis of functionally graded nanocomposite sandwich plates reinforced by defected CNT. Compos Struct 200:839–848. https://doi.org/10.1016/j.compstruct.2018.05.122
26. Thai CH, Ferreira AJM, Rabczuk T, Nguyen-Xuan H (2018) A naturally stabilized nodal integration meshfree formulation for carbon nanotube-reinforced composite plate analysis. Eng Anal Bound Elem 92:136–155. https://doi.org/10.1016/j.enganabound.2017.10.018
27. Ansari R, Torabi J, Hassani R (2019) A comprehensive study on the free vibration of arbitrary shaped thick functionally graded CNT-reinforced composite plates. Eng Struct 181:653–669. https://doi.org/10.1016/j.engstruct.2018.12.049
28. Chakraborty S, Dey T, Kumar R (2019) Stability and vibration analysis of CNT-reinforced functionally graded laminated composite cylindrical shell panels using semi-analytical approach. Compos B Eng 168:1–14. https://doi.org/10.1016/j.compositesb.2018.12.051
29. Ebrahimi F, Farazmandnia N, Kokaba MR, Mahesh V (2019) Vibration analysis of porous magneto-electro-elastically actuated carbon nanotube-reinforced composite sandwich plate based on a refined plate theory. Eng Comput. https://doi.org/10.1007/s00366-019-00864-4
30. Jiao P, Chen Z, Li Y, Ma H, Wu J (2019) Dynamic buckling analyses of functionally graded carbon nanotubes reinforced composite (FG-CNTRC) cylindrical shell under axial power-law time-varying displacement load. Compos Struct 220:784–797. https://doi.org/10.1016/j.compstruct.2019.04.048
31. Khosravi S, Arvin H, Kiani Y (2019) Interactive thermal and inertial buckling of rotating temperature-dependent FG-CNT reinforced composite beams. Compos B Eng 175:107178. https://doi.org/10.1016/j.compositesb.2019.107178
32. Mehar K, Panda SK (2019) Theoretical deflection analysis of multi-walled carbon nanotube reinforced sandwich panel and experimental verification. Compos B Eng 167:317–328. https://doi.org/10.1016/j.compositesb.2018.12.058
33. Ghorbanpour Arani A, Kiani F, Afshari H (2020) Free and forced vibration analysis of laminated functionally graded CNT-reinforced composite cylindrical panels. J Sandw Struct Mater. https://doi.org/10.1177/1099636219830787
34. Civalek Ö, Avcar M (2020) Free vibration and buckling analyses of CNT reinforced laminated non-rectangular plates by discrete singular convolution method. Eng Comput. https://doi.org/10.1007/s00366-020-01168-8
35. Moradi-Dastjerdi R, Behdinan K, Safaei B, Qin Z (2020) Buckling behavior of porous CNT-reinforced plates integrated between active piezoelectric layers. Eng Struct 222:111141. https://doi.org/10.1016/j.engstruct.2020.111141
36. Zhang M, Li J (2009) Carbon nanotube in different shapes. Mater Today 12(6):12–18. https://doi.org/10.1016/S1369-7021(09)70176-2
37. Ebrahimi F, Dabbagh A (2020) A brief review on the influences of nanotubes' entanglement and waviness on the mechanical behaviors of CNTR polymer nanocomposites. J Comput Appl Mech 51(1):247–252. https://doi.org/10.22059/jcamech.2020.304476.517
38. Arasteh R, Omidi M, Rousta AHA, Kazerooni H (2011) A study on effect of waviness on mechanical properties of multi-walled carbon nanotube/epoxy composites using modified Halpin–Tsai theory. J Macromol Sci Part B 50(12):2464–2480. https://doi.org/10.1080/00222348.2011.579868
39. Tornabene F, Fantuzzi N, Bacciocchi M, Viola E (2016) Effect of agglomeration on the natural frequencies of functionally graded carbon nanotube-reinforced laminated composite doubly-curved shells. Compos B Eng 89:187–218. https://doi.org/10.1016/j.compositesb.2015.11.016
40. Bacciocchi M, Tarantino AM (2019) Time-dependent behavior of viscoelastic three-phase composite plates reinforced by carbon nanotubes. Compos Struct 216:20–31. https://doi.org/10.1016/j.compstruct.2019.02.083
41. Rafiee M, Liu XF, He XQ, Kitipornchai S (2014) Geometrically nonlinear free vibration of shear deformable piezoelectric carbon nanotube/fiber/polymer multiscale laminated composite plates. J Sound Vib 333(14):3236–3251. https://doi.org/10.1016/j.jsv.2014.02.033

42. He XQ, Rafiee M, Mareishi S, Liew KM (2015) Large amplitude vibration of fractionally damped viscoelastic CNTs/fiber/polymer multiscale composite beams. Compos Struct 131:1111–1123. https://doi.org/10.1016/j.compstruct.2015.06.038
43. Rafiee M, Nitzsche F, Labrosse M (2016) Rotating nanocomposite thin-walled beams undergoing large deformation. Compos Struct 150:191–199. https://doi.org/10.1016/j.compstruct.2016.05.014
44. Ebrahimi F, Habibi S (2018) Nonlinear eccentric low-velocity impact response of a polymer-carbon nanotube-fiber multiscale nanocomposite plate resting on elastic foundations in hygrothermal environments. Mech Adv Mater Struct 25(5):425–438. https://doi.org/10.1080/15376494.2017.1285453
45. Rafiee M, Nitzsche F, Labrosse MR (2018) Modeling and mechanical analysis of multiscale fiber-reinforced graphene composites: nonlinear bending, thermal post-buckling and large amplitude vibration. Int J Non-Linear Mech 103:104–112. https://doi.org/10.1016/j.ijnonlinmec.2018.05.004
46. Rafiee M, Nitzsche F, Laliberte J, Hind S, Robitaille F, Labrosse MR (2019) Thermal properties of doubly reinforced fiberglass/epoxy composites with graphene nanoplatelets, graphene oxide and reduced-graphene oxide. Compos B Eng 164:1–9. https://doi.org/10.1016/j.compositesb.2018.11.051
47. Ebrahimi F, Dabbagh A (2019) Vibration analysis of graphene oxide powder-/carbon fiber-reinforced multi-scale porous nanocomposite beams: a finite-element study. Eur Phys J Plus 134(5):225. https://doi.org/10.1140/epjp/i2019-12594-1
48. Ebrahimi F, Dabbagh A (2021) An analytical solution for static stability of multi-scale hybrid nanocomposite plates. Eng Comput 37(1):545–559. https://doi.org/10.1007/s00366-019-00840-y
49. Ebrahimi F, Dabbagh A, Rastgoo A (2019) Free vibration analysis of multi-scale hybrid nanocomposite plates with agglomerated nanoparticles. Mech Based Design Struct Mach. https://doi.org/10.1080/15397734.2019.1692665
50. Ebrahimi F, Seyfi A, Dabbagh A (2019) Wave dispersion characteristics of agglomerated multi-scale hybrid nanocomposite beams. J Strain Anal Eng Design 54(4):276–289. https://doi.org/10.1177/0309324719862713
51. Dabbagh A, Rastgoo A, Ebrahimi F (2020) Static stability analysis of agglomerated multi-scale hybrid nanocomposites via a refined theory. Eng Comput. https://doi.org/10.1007/s00366-020-00939-7
52. Dabbagh A, Rastgoo A, Ebrahimi F (2020) Post-buckling analysis of imperfect multi-scale hybrid nanocomposite beams rested on a nonlinear stiff substrate. Eng Comput. https://doi.org/10.1007/s00366-020-01064-1
53. Ebrahimi F, Dabbagh A (2020) Vibration analysis of multi-scale hybrid nanocomposite shells by considering nanofillers' aggregation. Waves Random Complex Media. https://doi.org/10.1080/17455030.2020.1810363
54. Ebrahimi F, Dabbagh A, Rastgoo A, Rabczuk T (2020) Agglomeration effects on static stability analysis of multi-scale hybrid nanocomposite plates. Comput Mater Contin 63(1):41–64. https://doi.org/10.32604/cmc.2020.07947
55. Dabbagh A, Rastgoo A, Ebrahimi F (2021) Thermal buckling analysis of agglomerated multiscale hybrid nanocomposites via a refined beam theory. Mech Based Des Struct Mach 49(3):403–429. https://doi.org/10.1080/15397734.2019.1692666
56. Ebrahimi F, Dabbagh A (2021) Vibration analysis of fluid-conveying multi-scale hybrid nanocomposite shells with respect to agglomeration of nanofillers. Def Technol 17(1):212–225. https://doi.org/10.1016/j.dt.2020.01.007
57. Ferry JD (1980) Viscoelastic properties of polymers, 3rd edn. Wiley
58. Drozdov AD, Kalamkarov AL (1996) A constitutive model for nonlinear viscoelastic behavior of polymers. Polym Eng Sci 36(14):1907–1919. https://doi.org/10.1002/pen.10587
59. Brinson HF, Brinson LC (2008) Polymer engineering science and viscoelasticity, 2nd edn. Springer, Boston. https://doi.org/10.1007/978-1-4899-7485-3
60. Cox HL (1952) The elasticity and strength of paper and other fibrous materials. Br J Appl Phys 3(3):72–79. https://doi.org/10.1088/0508-3443/3/3/302
61. Thai CH, Kulasegaram S, Tran LV, Nguyen-Xuan H (2014) Generalized shear deformation theory for functionally graded isotropic and sandwich plates based on isogeometric approach. Comput Struct 141:94–112. https://doi.org/10.1016/j.compstruc.2014.04.003
62. Nguyen TN, Thai CH, Nguyen-Xuan H (2016) On the general framework of high order shear deformation theories for laminated composite plate structures: a novel unified approach. Int J Mech Sci 110:242–255. https://doi.org/10.1016/j.ijmecsci.2016.01.012
63. Ebrahimi F, Dabbagh A (2019) Wave propagation analysis of smart nanostructures, 1st edn. CRC Press, Boca Raton. https://doi.org/10.1201/9780429279225
64. Zaoui FZ, Ouinas D, Tounsi A (2019) New 2D and quasi-3D shear deformation theories for free vibration of functionally graded plates on elastic foundations. Compos B Eng 159:231–247. https://doi.org/10.1016/j.compositesb.2018.09.051
65. Ebrahimi F, Dabbagh A (2020) Mechanics of nanocomposites: homogenization and analysis, 1st edn. CRC Press, Boca Raton. https://doi.org/10.1201/9780429316791
66. Nguyen TN, Ngo TD, Nguyen-Xuan H (2017) A novel three-variable shear deformation plate formulation: theory and isogeometric implementation. Comput Methods Appl Mech Eng 326:376–401. https://doi.org/10.1016/j.cma.2017.07.024
67. Ebrahimi F, Dabbagh A (2018) Effect of humid-thermal environment on wave dispersion characteristics of single-layered graphene sheets. Appl Phys A 124(4):301. https://doi.org/10.1007/s00339-018-1734-y
68. Ebrahimi F, Dabbagh A (2018) On wave dispersion characteristics of double-layered graphene sheets in thermal environments. J Electromagn Waves Appl 32(15):1869–1888. https://doi.org/10.1080/09205071.2017.1417918
69. Ebrahimi F, Dabbagh A (2019) Vibration analysis of multi-scale hybrid nanocomposite plates based on a Halpin–Tsai homogenization model. Compos B Eng 173:106955. https://doi.org/10.1016/j.compositesb.2019.106955
70. Ebrahimi F, Dabbagh A (2019) On thermo-mechanical vibration analysis of multi-scale hybrid composite beams. J Vib Control 25(4):933–945. https://doi.org/10.1177/1077546318806800
71. Ebrahimi F, Dabbagh A, Civalek Ö (2019) Vibration analysis of magnetically affected graphene oxide-reinforced nanocomposite beams. J Vib Control 25(23–24):2837–2849. https://doi.org/10.1177/1077546319861002
72. Ebrahimi F, Dabbagh A, Rastgoo A (2019) Vibration analysis of porous metal foam shells rested on an elastic substrate. J Strain Anal Eng Design 54(3):199–208. https://doi.org/10.1177/0309324719852555
73. Ebrahimi F, Seyfi A, Dabbagh A, Tornabene F (2019) Wave dispersion characteristics of porous graphene platelet-reinforced composite shells. Struct Eng Mech 71(1):99–107. https://doi.org/10.12989/sem.2019.71.1.099
74. Mishra BP, Barik M (2019) NURBS-augmented finite element method for stability analysis of arbitrary thin plates. Eng Comput 35(2):351–362. https://doi.org/10.1007/s00366-018-0603-9
75. Nguyen TN, Thai CH, Luu A-T, Nguyen-Xuan H, Lee J (2019) NURBS-based postbuckling analysis of functionally graded carbon nanotube-reinforced composite shells. Comput Methods Appl Mech Eng 347:983–1003. https://doi.org/10.1016/j.cma.2019.01.011
76. Zhang C, Gholipour G, Mousavi AA (2019) Nonlinear dynamic behavior of simply-supported RC beams subjected to combined

impact-blast loading. Eng Struct 181:124–142. https://doi.org/10.1016/j.engstruct.2018.12.014
77. Cao Y, Musharavati F, Baharom S, Talebizadehsardari P, Sebaey TA, Eyvazian A (2020) Vibration response of FG-CNT-reinforced plates covered by magnetic layer utilizing numerical solution. Steel Compos Struct 37(2):253–258. https://doi.org/10.12989/scs.2020.37.2.253
78. Dastjerdi S, Akgöz B, Civalek Ö (2020) On the effect of viscoelasticity on behavior of gyroscopes. Int J Eng Sci 149:103236. https://doi.org/10.1016/j.ijengsci.2020.103236
79. Ebrahimi F, Barati MR, Civalek Ö (2020) Application of Chebyshev–Ritz method for static stability and vibration analysis of nonlocal microstructure-dependent nanostructures. Eng Comput 36(3):953–964. https://doi.org/10.1007/s00366-019-00742-z
80. Ebrahimi F, Dabbagh A, Rastgoo A (2020) Static stability analysis of multi-scale hybrid agglomerated nanocomposite shells. Mech Based Design Struct Mach. https://doi.org/10.1080/15397734.2020.1848585
81. Ebrahimi F, Nouraei M, Dabbagh A (2020) Modeling vibration behavior of embedded graphene-oxide powder-reinforced nanocomposite plates in thermal environment. Mech Based Des Struct Mach 48(2):217–240. https://doi.org/10.1080/15397734.2019.1660185
82. Ebrahimi F, Nouraei M, Dabbagh A (2020) Thermal vibration analysis of embedded graphene oxide powder-reinforced nanocomposite plates. Eng Comput 36(3):879–895. https://doi.org/10.1007/s00366-019-00737-w
83. Eyvazian A, Musharavati F, Talebizadehsardari P, Sebaey TA (2020) Free vibration of FG-GPLRC spherical shell on two parameter elastic foundation. Steel Compos Struct 36(6):711–727. https://doi.org/10.12989/scs.2020.36.6.711
84. Eyvazian A, Musharavati F, Tarlochan F, Pasharavesh A, Rajak DK, Husain MB, Tran TN (2020) Free vibration of FG-GPLRC conical panel on elastic foundation. Struct Eng Mech 75(1):1–18. https://doi.org/10.12989/sem.2020.75.1.001
85. Eyvazian A, Shahsavari D, Karami B (2020) On the dynamic of graphene reinforced nanocomposite cylindrical shells subjected to a moving harmonic load. Int J Eng Sci 154:103339. https://doi.org/10.1016/j.ijengsci.2020.103339
86. Khorasani M, Eyvazian A, Karbon M, Tounsi A, Lampani L, Sebaey TA (2020) Magneto-electro-elastic vibration analysis of modified couple stress-based three-layered micro rectangular plates exposed to multi-physical fields considering the flexoelectricity effects. Smart Struct Syst 26(3):331–343. https://doi.org/10.12989/sss.2020.26.3.331
87. Talebizadehsardari P, Eyvazian A, Gorji Azandariani M, Tran TN, Rajak DK, Babaei Mahani R (2020) Buckling analysis of smart beams based on higher order shear deformation theory and numerical method. Steel Compos Struct 35(5):635–640. https://doi.org/10.12989/scs.2020.35.5.635
88. Talebizadehsardari P, Eyvazian A, Musharavati F, Babaei Mahani R, Sebaey TA (2020) Elastic wave characteristics of graphene reinforced polymer nanocomposite curved beams including thickness stretching effect. Polymers 12(10):2194. https://doi.org/10.3390/polym12102194
89. Yarali E, Farajzadeh MA, Noroozi R, Dabbagh A, Khoshgoftar MJ, Mirzaali MJ (2020) Magnetorheological elastomer composites: modeling and dynamic finite element analysis. Compos Struct 254:112881. https://doi.org/10.1016/j.compstruct.2020.112881
90. Civalek Ö, Dastjerdi S, Akbaş ŞD, Akgöz B (2021) Vibration analysis of carbon nanotube-reinforced composite microbeams. Math Methods Appl Sci. https://doi.org/10.1002/mma.7069
91. Ebrahimi F, Dabbagh A, Rabczuk T (2021) On wave dispersion characteristics of magnetostrictive sandwich nanoplates in thermal environments. Eur J Mech A Solids 85:104130. https://doi.org/10.1016/j.euromechsol.2020.104130
92. Motezaker M, Eyvazian A (2020) Buckling load optimization of beam reinforced by nanoparticles. Struct Eng Mech 73(5):481–486. https://doi.org/10.12989/sem.2020.73.5.481
93. Song M, Kitipornchai S, Yang J (2017) Free and forced vibrations of functionally graded polymer composite plates reinforced with graphene nanoplatelets. Compos Struct 159:579–588. https://doi.org/10.1016/j.compstruct.2016.09.070
94. García-Macías E, Rodríguez-Tembleque L, Sáez A (2018) Bending and free vibration analysis of functionally graded graphene vs. carbon nanotube reinforced composite plates. Compos Struct 186:123–138. https://doi.org/10.1016/j.compstruct.2017.11.076
95. Wattanasakulpong N, Chaikittiratana A (2015) Exact solutions for static and dynamic analyses of carbon nanotube-reinforced composite plates with Pasternak elastic foundation. Appl Math Model 39(18):5459–5472. https://doi.org/10.1016/j.apm.2014.12.058

Terms and Conditions

Springer Nature journal content, brought to you courtesy of Springer Nature Customer Service Center GmbH (“Springer Nature”).
Springer Nature supports a reasonable amount of sharing of research papers by authors, subscribers and authorised users (“Users”), for small-scale personal, non-commercial use provided that all copyright, trade and service marks and other proprietary notices are maintained. By accessing, sharing, receiving or otherwise using the Springer Nature journal content you agree to these terms of use (“Terms”). For these purposes, Springer Nature considers academic use (by researchers and students) to be non-commercial.
These Terms are supplementary and will apply in addition to any applicable website terms and conditions, a relevant site licence or a personal subscription. These Terms will prevail over any conflict or ambiguity with regards to the relevant terms, a site licence or a personal subscription (to the extent of the conflict or ambiguity only). For Creative Commons-licensed articles, the terms of the Creative Commons license used will apply.
We collect and use personal data to provide access to the Springer Nature journal content. We may also use these personal data internally within ResearchGate and Springer Nature and as agreed share it, in an anonymised way, for purposes of tracking, analysis and reporting. We will not otherwise disclose your personal data outside the ResearchGate or the Springer Nature group of companies unless we have your permission as detailed in the Privacy Policy.
While Users may use the Springer Nature journal content for small scale, personal non-commercial use, it is important to note that Users may not:

1. use such content for the purpose of providing other users with access on a regular or large scale basis or as a means to circumvent access control;
2. use such content where to do so would be considered a criminal or statutory offence in any jurisdiction, or gives rise to civil liability, or is otherwise unlawful;
3. falsely or misleadingly imply or suggest endorsement, approval , sponsorship, or association unless explicitly agreed to by Springer Nature in writing;
4. use bots or other automated methods to access the content or redirect messages
5. override any security feature or exclusionary protocol; or
6. share the content in order to create substitute for Springer Nature products or services or a systematic database of Springer Nature journal content.

In line with the restriction against commercial use, Springer Nature does not permit the creation of a product or service that creates revenue, royalties, rent or income from our content or its inclusion as part of a paid for service or for other commercial gain. Springer Nature journal content cannot be used for inter-library loans and librarians may not upload Springer Nature journal content on a large scale into their, or any other, institutional repository.
These terms of use are reviewed regularly and may be amended at any time. Springer Nature is not obligated to publish any information or content on this website and may remove it or features or functionality at our sole discretion, at any time with or without notice. Springer Nature may revoke this licence to you at any time and remove access to any copies of the Springer Nature journal content which have been saved.
To the fullest extent permitted by law, Springer Nature makes no warranties, representations or guarantees to Users, either express or implied with respect to the Springer nature journal content and all parties disclaim and waive any implied warranties or warranties imposed by law, including merchantability or fitness for any particular purpose.
Please note that these rights do not automatically extend to content, data or other material published by Springer Nature that may be licensed from third parties.
If you would like to use or distribute our Springer Nature journal content to a wider audience or on a regular basis or in any other manner not expressly permitted by these Terms, please contact Springer Nature at

onlineservice@springernature.com